Supporting Information

Stabilizing doped Spiro-OMeTAD by organic molten salt for efficient and stable perovskite solar cells

Tengfei Pan,[1] Zhiwei Li,[1] Biyun Ren,[1] Wan Yang,[1] Xueqin Ran,[1] Yajing Li,[1] Yutian Xu,[1] Yue Wang,[2] Deli Li,[2] Yingdong Xia,[1] Xingyu Gao,[3] Lingfeng Chao,[1*] Yonghua Chen[1*]

[1]Key Laboratory of Flexible Electronics (KLoFE) & Institute of Advanced Materials (IAM), School of Flexible Electronics (Future Technologies), Nanjing Tech University (NanjingTech), 30 South Puzhu Road, Nanjing 211816, Jiangsu, China.

[2]Fujian Cross Strait Institute of Flexible Electronics (Future Technologies), Fujian Normal University, Fuzhou 350117, China.

[3]Shanghai Synchrotron Radiation Facility, Shanghai Institute of Applied Physics, Chinese Academy of Sciences, Shanghai 201204, P. R. China.

Tengfei Pan and Zhiwei Li contribute equally.

*Corresponding author. Email: iamlfchao@njtech.edu.cn (L.C.);

iamyhchen@njtech.edu.cn (Y.C.)

Materials and Methods

Materials

SnO_2 colloid precursor (tin (iv) oxide, 15% in H_2O colloidal dispersion) was purchased from Alfa Aesar. PbI_2 (Lead iodide); Spiro-OMeTAD (2, 2', 7, 7'-tetrakis(N, N-di-p-methoxy-phenylamine)-9, 9'-spirobifuorene) were purchased from Advanced Election Technology Company in China. FAI (formamidinium iodide), MACl (mthylammonium chloride) was purchased from Great Cell. CY (cyclohexylamine), TFA (trifluoroacetic acid), Ac (acetic acid), DMSO (dimethyl sulfoxide), DMF (N, N-dimethylformamide), tBP (4-tert-butyl pyridine), CB (chlorobenzene), OAI (n-Octylammonium Iodide), LiTFSI (lithium bis(trifluoromethanesulfonyl)imide), IPA (isopropyl alcohol) and were purchased from Sigma-Aldrich. CYI (Cyclohexylamine Hydroiodide) were purchased from Aladdin.

Synthesis of CYTFA

Solution A: Put 8 ml of trifluoroacetic acid into a beaker, and then use 50 ml of anhydrous methanol for dilution. Solution B put 35 ml Cyclohexylamine (33% ethanol solution) into the flask, stir at -16°C, and then dilute with 60 ml of absolute ethanol. After the temperature of solution B is stabilized, solution A is slowly added drop wise to solution B. It is worth noting that during this process, solution B was kept at -16 °C and continuously stirred. Finally, after continuous stirring for 2 hours, the solution was subjected to rotary evaporation at 55 °C to remove the remaining solvent to obtain the product CYTFA.

Synthesis of CYAc

Solution A: Put 6 ml of acetic acid into a beaker, and then use 50 ml of anhydrous methanol for dilution. Solution B put 12 ml Cyclohexylamine (33% ethanol solution) into the flask, stir at -16°C, and then dilute with 60 ml of absolute ethanol. The subsequent synthesis steps are the same as CYTFA.

Doping methodology

The organic molten salt doping of spiro-OMeTAD was prepared by dissolving 72.3 mg spiro-OMeTAD in 1 mL CB and doped with 25 μL LiTFSI salt in acetonitrile (520 mg mL^{-1}) and 35 μL TBP with different loading of CYTFA, and stirred at room temperature overnight.

Device fabrication

FTO substrates were ultrasonic cleaned sequentially in deionized water and isopropanol for 30 min respectively, and dried by a compressed nitrogen gun. After 30 min UV-Ozone surface treatment, we deposited SnO_2 ETL by spin coating a 1:3 diluted SnO_2 nanoparticle water solution at 4,000 rpm for 30 s, followed by annealing at 150 °C for 20 min in air. Afterwards, a thin potassium chloride (KCl, 99 %, Sigma-Aldrich) layer was deposited by spin coating 1 mg ml^{-1} KCl deionized water solution at 3,000 rpm for 30 s and annealed at 100 °C for 10 min in air. The perovskite $FAPbI_3$ active layer precursor was prepared by mixing 1.81 M PbI_2, 1.8M FAI, 0.42M MACL, and dissolved in anhydrous DMF and DMSO with the volume ratio of 8:1 mixed solution. For the recipe with 1 mg mL^{-1} Potassium Iodide (KI, ≥99%, Sigma-Aldrich) was added into the perovskite precursors as additive. The perovskite solution was then deposited via spin coating at 5000 rpm for 30 sec (2,000 rpm ramp). Within 10 s of the 5,000-rpm spinning, 1mL of diethyl ether as the antisolvent was deposited onto the film. After spin-coating, the perovskite film was then annealed at 150 °C for 15 min in ambient air. Then the 5 mg mL^{-1} OAI solution in IPA was spin-coated onto the perovskite surface at 5000 rpm and annealed at 100 °C for 1 min. Later, the different hole transport layers were deposited by spin coating at 5,000 rpm for 30 s without further annealing. Metal electrode of 80 nm Au was deposited on hole transporting layer through thermal evaporation method under a vacuum degree higher than 5×10^{-4} Torr to accomplish the solar cell fabrication. The solar cells are naturally oxidized in a brown dryer for 22h, and the humidity is controlled at about 5%. A 0.05 cm^2 shadow mask was used to define the effective working area of the solar cells.

Characterizations and measurements

HTL film characterizations

Proton nuclear magnetic resonance (NMR) spectra were measured with a JOEL NMR spectrometer (JNM-ECZ400S, 400 MHz Japan).

Fourier Transform Infrared (FTIR) spectroscopy was characterized by FT/IR-6100 (Jasco).

Scanning electron microscopy (SEM) analysis was performed on a SU8010 electron microscope. SEM images were captured using a 5-kV acceleration voltage and an aperture size of 20 μm.

Time-of-flight secondary-ion mass spectrometry (TOF-SIMS) measurements were carried out to analyse the depth profile. A primary beam (Bi^{3+}) at 30 kV and sputter beam (Cs^{+}) at 1 kV were used for analysising positive and negative polarities.

Grazing-incidence wide-angle X-ray scattering (GIWAXS) was performed at the BL14BL beamline of the Shanghai Synchrotron Radiation Facility (SSRF) using X-ray with a wavelength of 1.24 Å.

Space-charge limited current (SCLC) measurements were used to determine the hole mobility of pristine and doped HTL films on a hole-only device (FTO/MoO_3 5nm /Spiro-OMeTAD 180nm/MoO_3 5nm /70nm Au). The MoO3 and Au layers were all deposited by thermal evaporation. The classic Mott-Gurney equation was used to determine the mobility: $J=9\mu_{\varepsilon}0\varepsilon_r V^2/(8d^3)$, where $\varepsilon_r \approx 8.26$ is the average dielectric constant of the blended film, ε_0 is the vacuum permittivity of the free space, μ is the hole mobility, V is the applied bias, and d is the film thickness.

Ultraviolet photoelectron spectroscopy (UPS) was measured by Thermo ESCALAB 250 with a non-monochromated He I_α photon source (hν = 21.22 eV).

Steady-state photoluminescence (PL) spectra and Time-resolved photoluminescence (TRPL) spectra were obtained by FLS1000. The excitation wavelength was set as 520 nm. The TRPL decay data were modeled by a biexponential formula: $Y=A_1\exp(-t/\tau_1) + A_2\exp(-t/\tau_2)$.

Device characterizations

Charge extraction (CE) was performed using PAIOS system under different illumination intensity (1–100 mW $cm^{-2)}$ with an illumination duration of 100 us. Integrating the extraction current over time yields the extracted charge. The extracted charge carrier density nCE is then calculated according to the following equation:

$$n\mathrm{CE} = \frac{1}{L_q}\left(\int j(t)d(t) - (V_\mathrm{a} - V_\mathrm{e})\, C_\mathrm{geom}\right)$$

where L is the perovskite thickness, q is the unit charge, te is the extraction time, j(t) is the transient current density, C_{geom} is the geometric capacitance, V_a is the voltage applied prior extraction (in most cases Voc), and V_e is the extraction voltage. The charge on the capacitance needs to be subtracted17 as only the charge carrier density inside the bulk is of interest.

Photo-charge extraction by linearly increasing voltage (photo-CELIV) measurements were performed using a pulsed Nd:YAG laser (Quantel Ultra) operated at 532 nm. The laser pulse generates charges in the solar cells, and a linearly increasing voltage pulse is applied after a short delay to extract the photogenerated charge. A small, steady-state offset voltage (similar to V_{bi}) is applied in forward bias to prevent the extraction of photogenerated charges during the delay between the laser pulse and the linearly increasing applied voltage pulse.

Intensity Modulated Photovoltage Spectroscopy (IMVS) measurements were made using a PAIOS system developed by Fluxim AG. These measurements were made at different open-circuit voltages by varying the light intensity of a white LED. The frequency range used for the measurements was 1-107 Hz. The AC light intensity perturbation was set to 10% of the DC light intensity.

Transient photocurrent (TPC) measurement was performed with a system excited by a 532 nm (1000 Hz, 3.2 ns) pulse laser.

Transient photovoltage (TPV) measurement was performed with the same

system excited by a 405 nm (50 Hz, 20 ms) pulse laser. A digital oscilloscope (Tektronix, D4105) was used to record the photocurrent or photovoltage decay process with a sampling resistor of 50 Ω or 1 MΩ, respectively.

Photo current-voltage (J-V) curves were measured by using 2400 Series Source Meter (Keithley Instruments) under a SS-F5-3A solar simulator (AM 1.5G, 100 mW cm^{-2}) (Enlitech) calibrated by a NREL standard Si cell, and no additional UV filter equipment was used. The measurements were carried out with the devices inside the glove box (<0.1 ppm O_2 and H_2O). To ensure the accuracy of the Jsc measured from JV scans, a mask with an aperture area of 0.05 cm^2 was covered during the measurement. The J-V curves were scanned by reverse (forward bias (1.3 V) → short circuit (-0.2 V)) or forward (short circuit (-0.2 V) → forward bias (1.3 V)) scan with scan rate of 50 mVs^{-1}, and 1 ms delay time.

Stability tests

In order to test the stability of the device, we placed the device without any encapsulation in a N_2-filled glovebox or for more than 2800 hours. The encapsulation of PSCs devices is using EVA as the encapsulant and using glass as the cover. For hygrothermal stability studies, the devices are stored in a temperature and controlled-humidity cabinet with a transparent glass door. The internal relative temperature and humidity were controlled at the required 55±1℃ and 55±3 % humidity. The J-V curves were recorded with a Keithley 2400 source meter and under one sun illumination (AM 1.5G, 100 mW cm^{-2}) equipped with 425 W collimated Xenon lamp (EnliTech SS-F5-3A), in which the light intensity was calibrated by the NREL certified silicon solar cell. The operational stability tests were carried out at the MPPT for the unencapsulated devices under AM1.5 illumination (100 mW cm^{-2}) in atmosphere N_2 at 30±5 ℃. The voltage at the MPPT was automatically applied, and the power output of the devices was tracked.

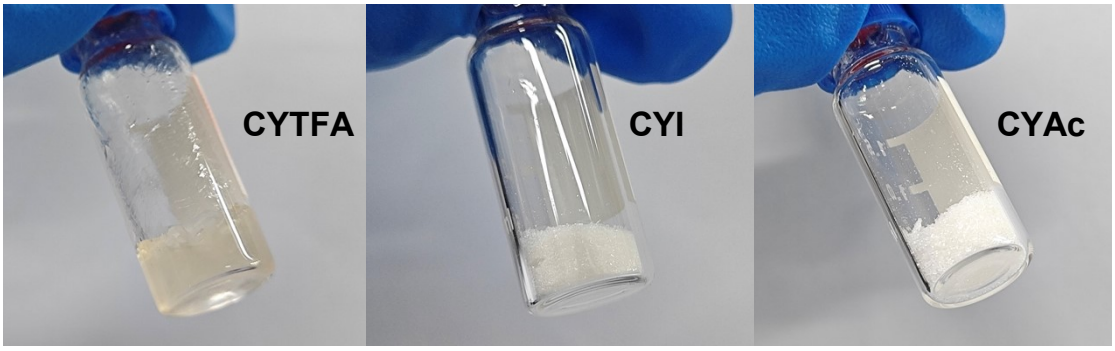

Fig. S1 Photographs of CYTFA, CYI, and CYAc at 150°C.

Fig. S2 Photographs of CYTFA, CYI, and CYAc at room temperature.

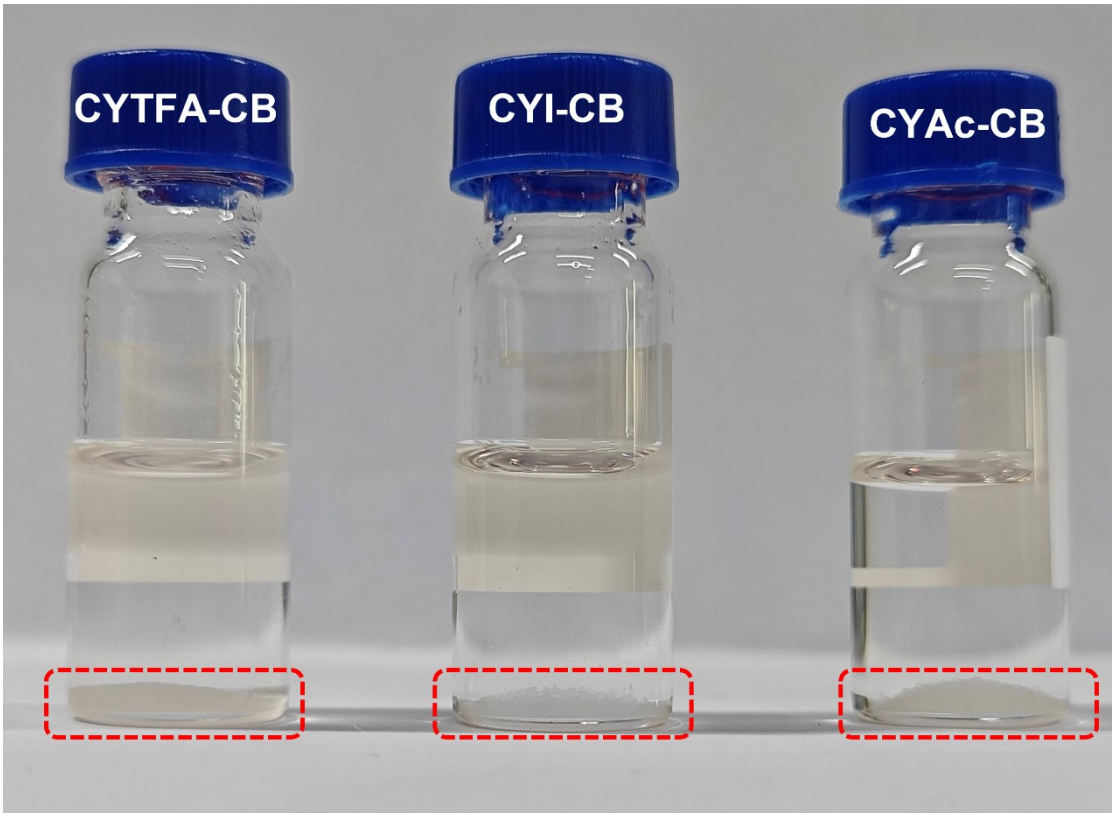

Fig. S3 Photographs of CYTFA, CYI, and CYAc in CB solutions.

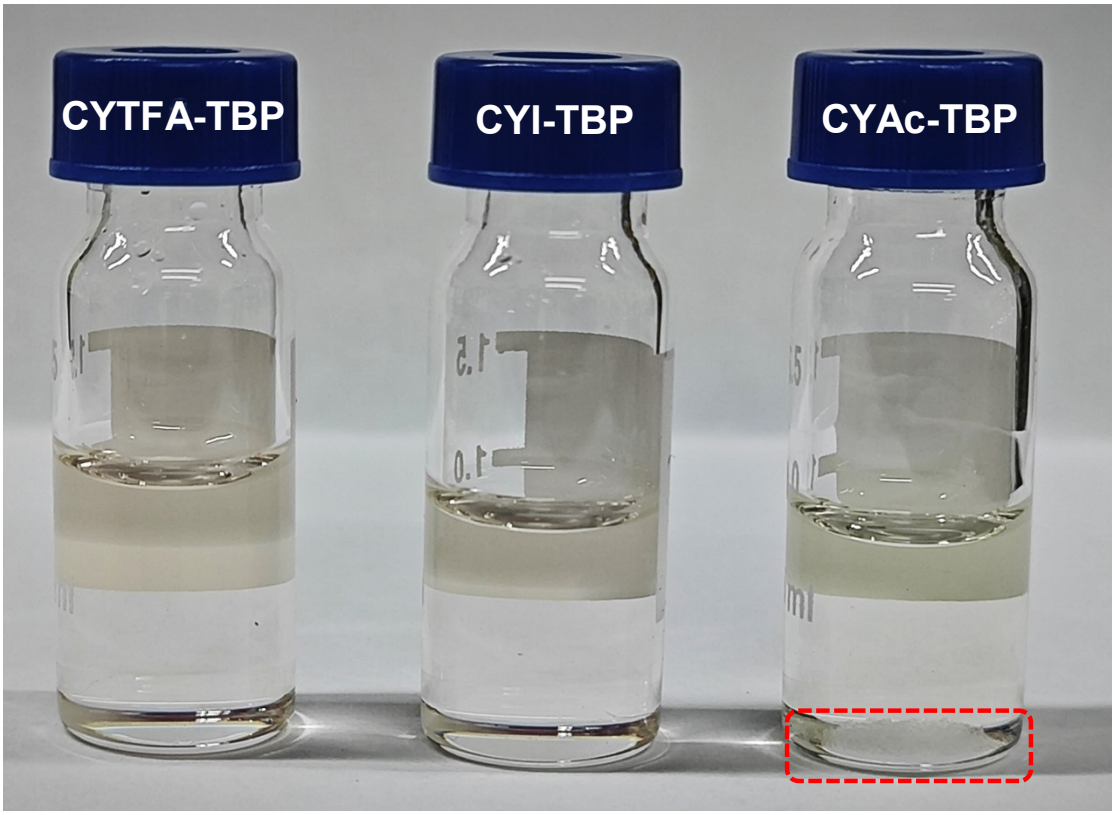

Fig. S4 Photographs of CYTFA, CYI, and CYAc in TBP solutions.

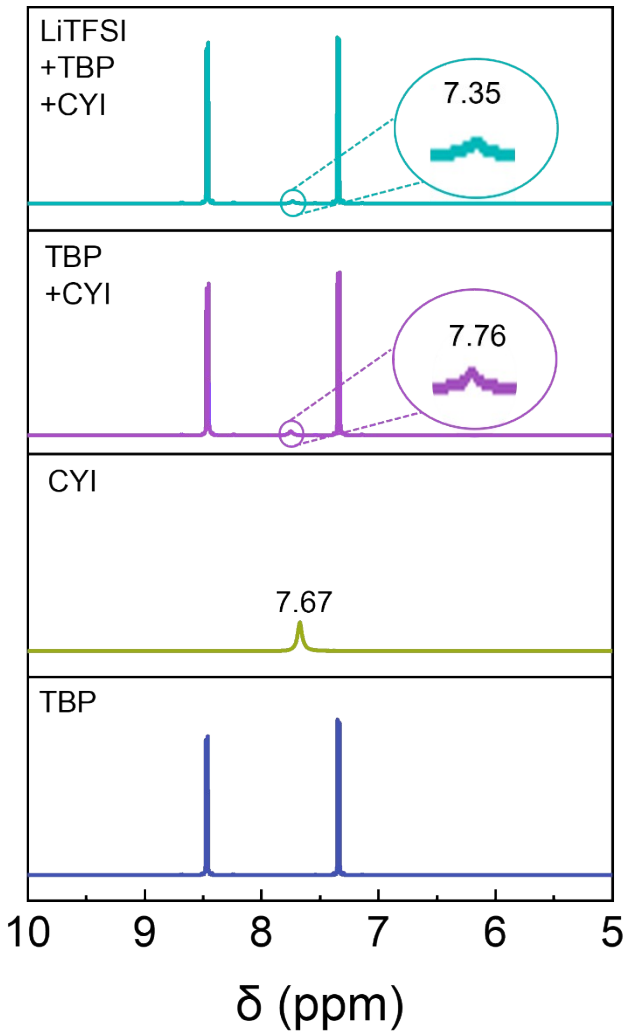

Fig. S5 ^{1}H NMR spectra of TBP, CYI, mixed solution of TBP and CYI, and mixed solution of TBP, CYI and LiTFSI.

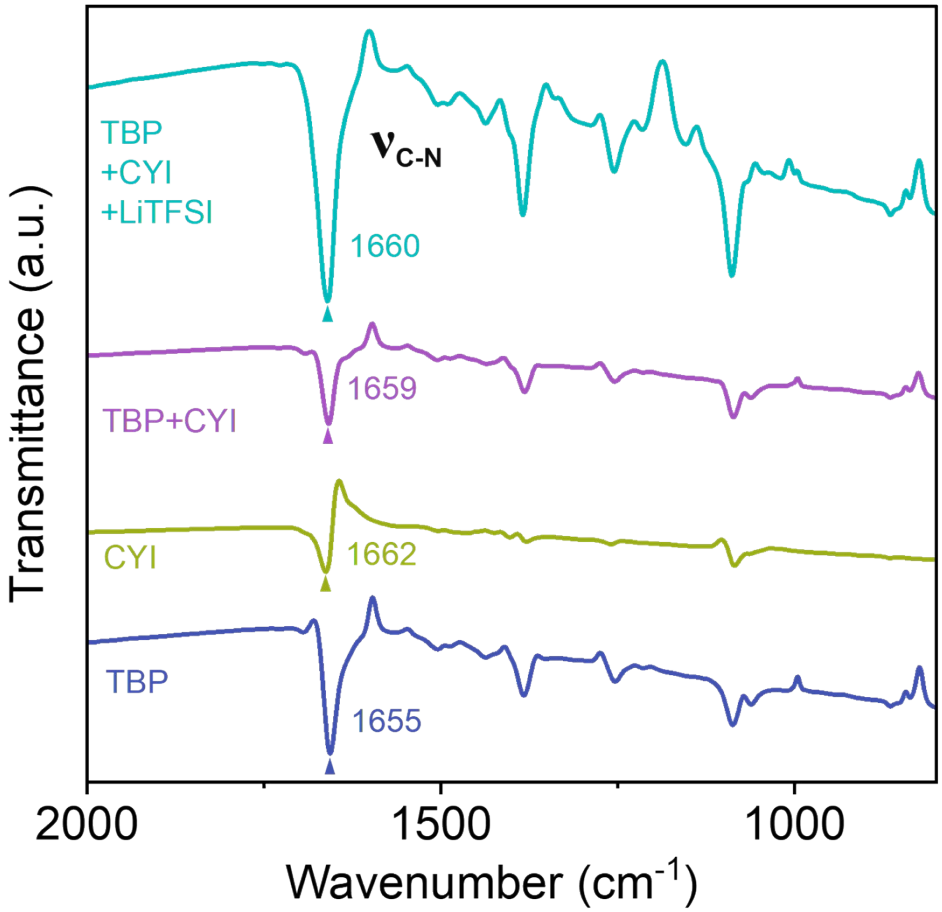

Fig. S6 FTIR spectra of TBP, CYI, mixed solution of TBP and CYI, and mixed solution of TBP, CYI and LiTFSI at the range of 800cm^{-1}-2000 cm^{-1}.

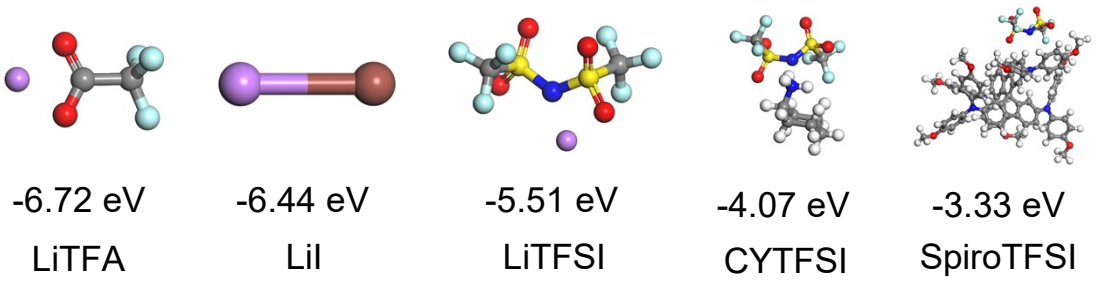

Fig. S7 Optimized molecular structures and binding energies of LiTFA, LiTFSI, CYTFSI, SpiroTFSI derived from density functional theory calculations.

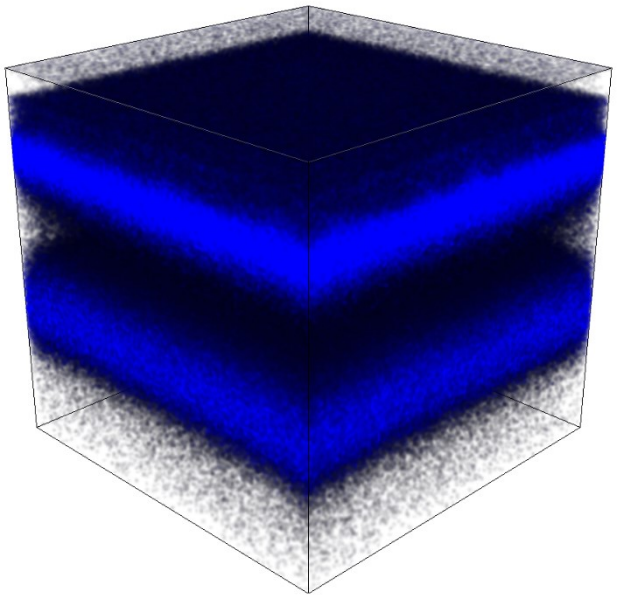

Fig. S8 TOF-SIMS for depth profiling and corresponding 3D distribution pictures of Li^+ in the CYI-Spiro device.

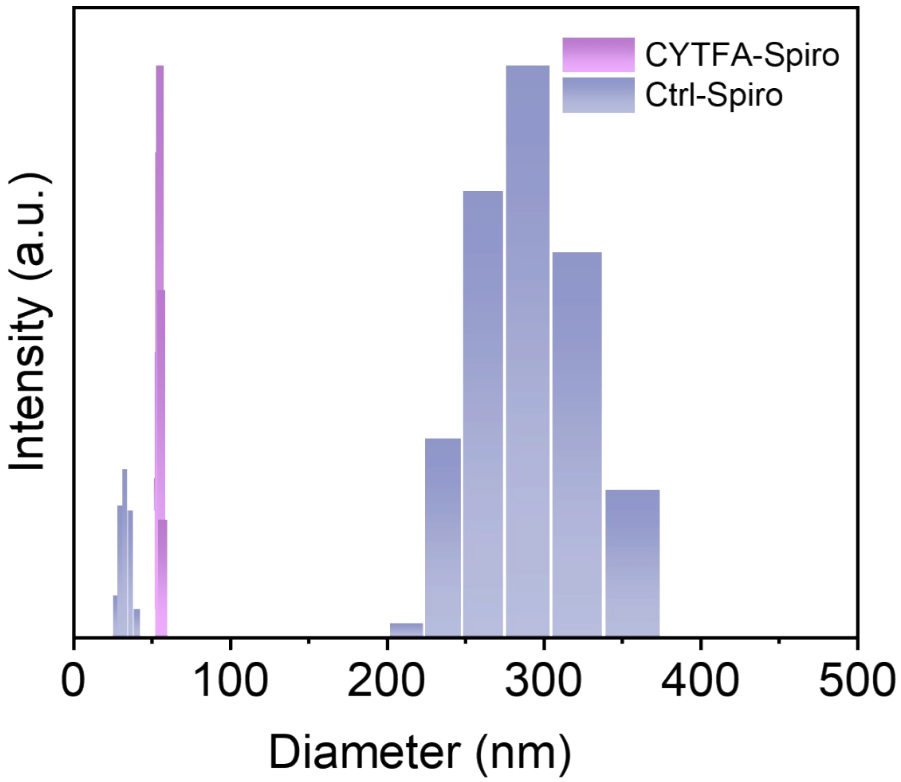

Fig. S9 Dynamic light scattering spectrum of CYTFA-Spiro and Ctrl-Spiro solution.

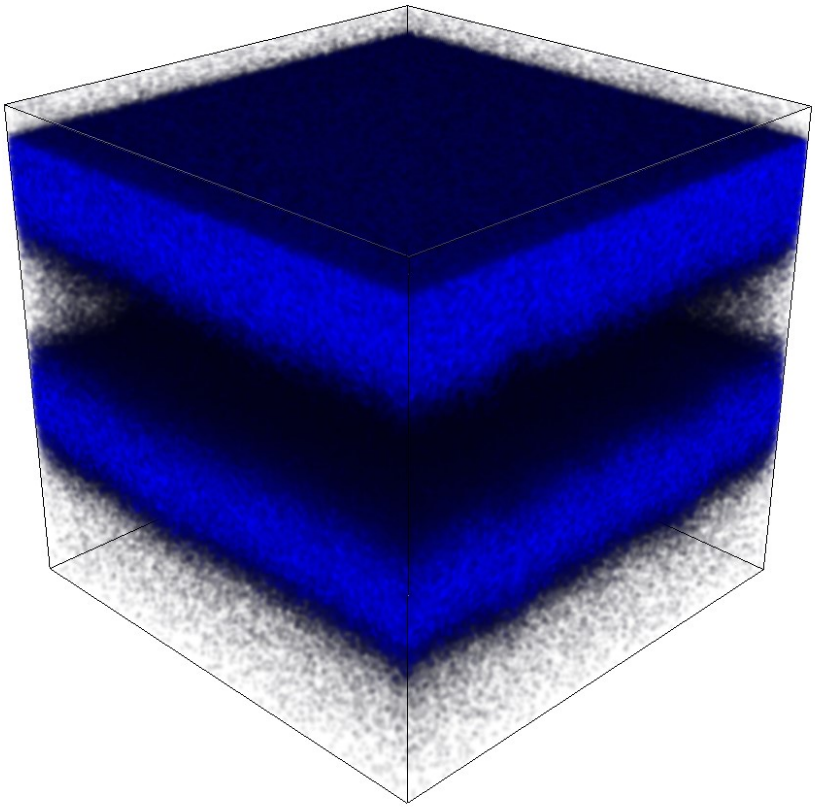

Fig. S10 TOF-SIMS for depth profiling and corresponding 3D distribution pictures of Li^+ in the Ctrl-Spiro device.

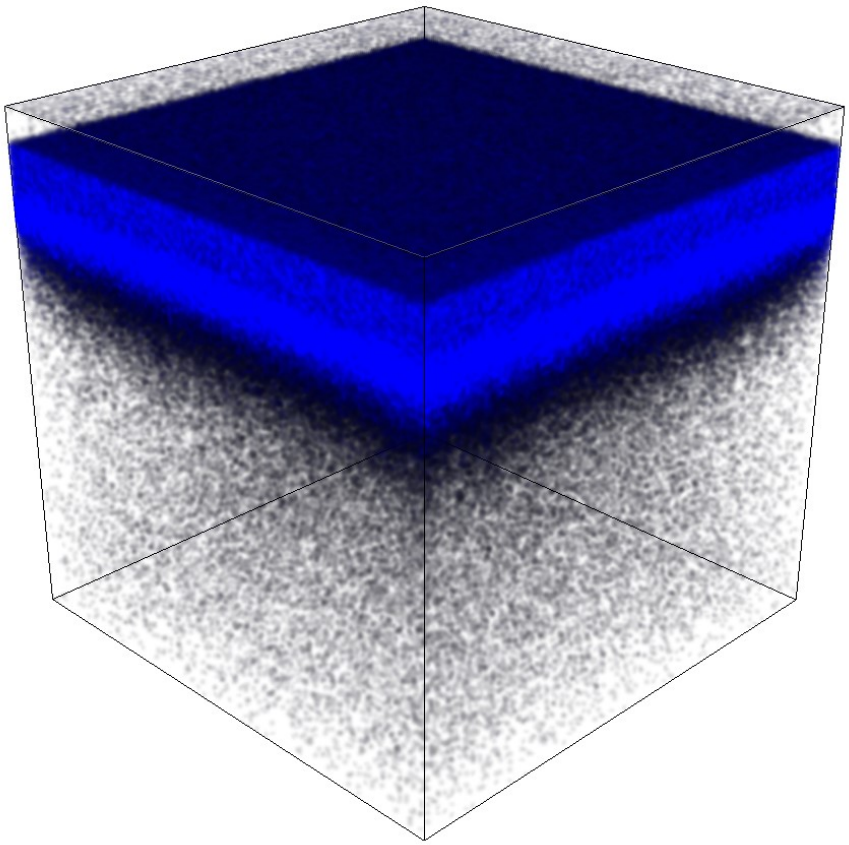

Fig. S11 TOF-SIMS for depth profiling and corresponding 3D distribution pictures of Li^+ in the CYTFA-Spiro device.

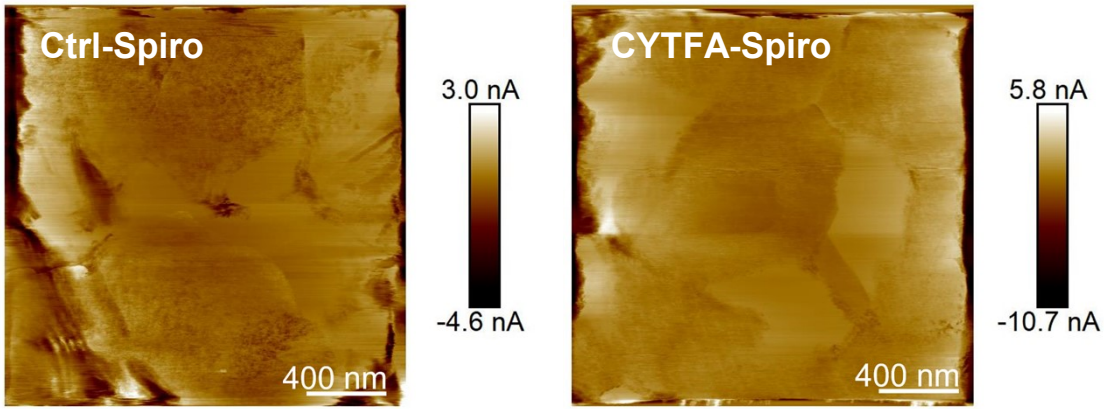

Fig. S12 C-AFM mapping of Ctrl-Spiro and CYTFA-Spiro thin films on perovskite layer.

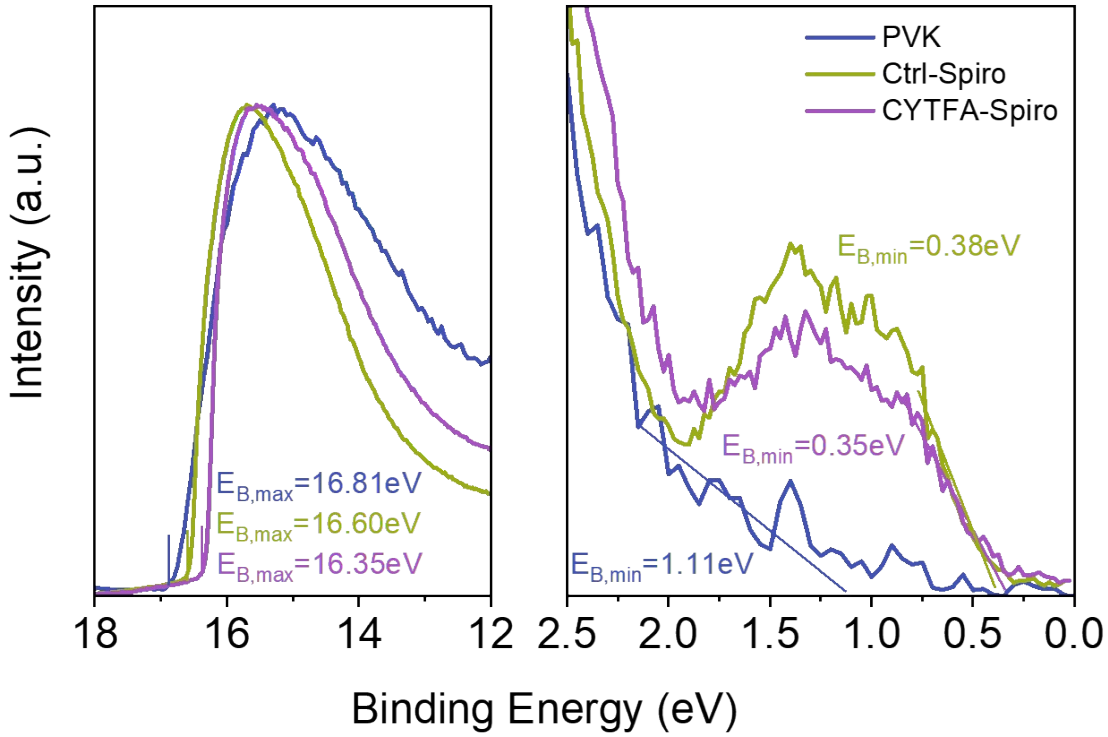

Fig. S13 UPS characterization of the perovskite, Ctrl-Spiro and CYTFA-Spiro thin films.

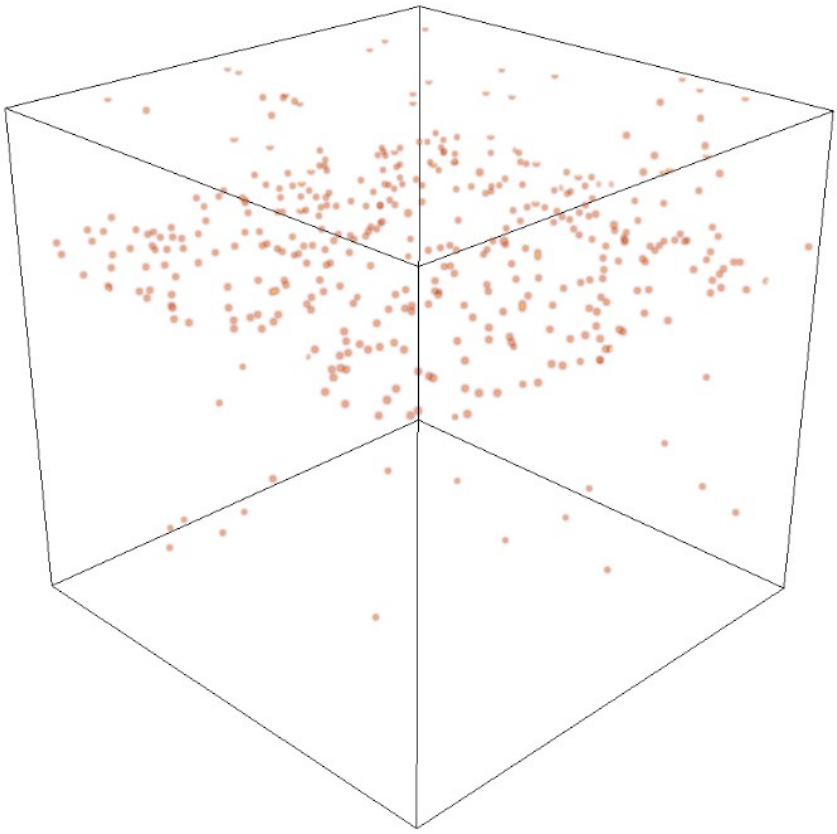

Fig. S14 TOF-SIMS for depth analyzing of CY^+ in CYTFA-Spiro device.

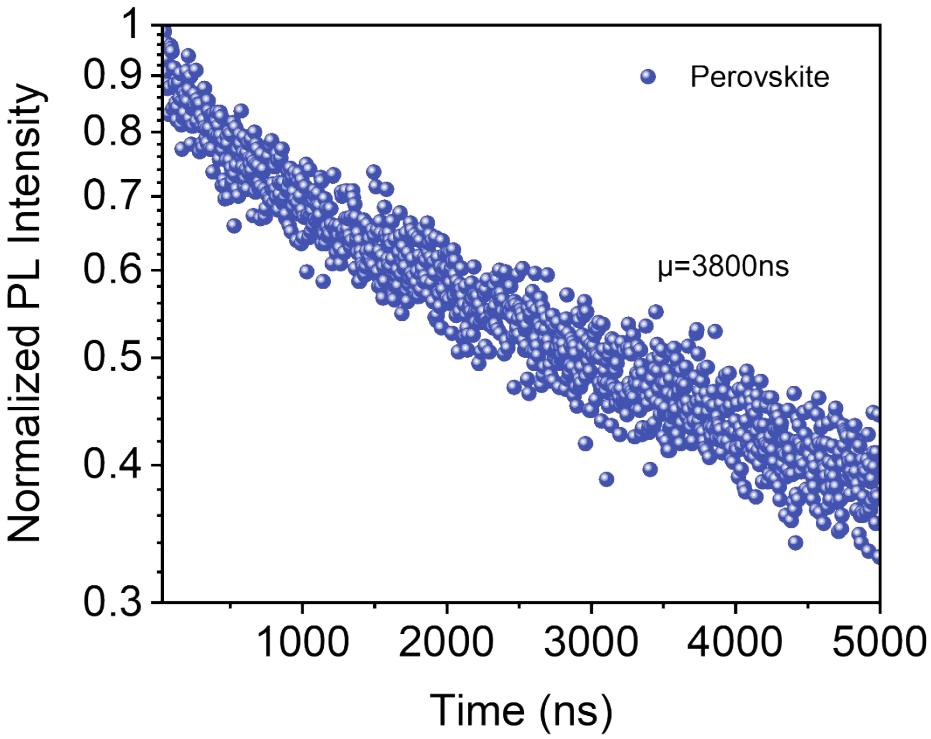

Fig. S15 TRPL spectra of the perovskite deposited on glass substrates.

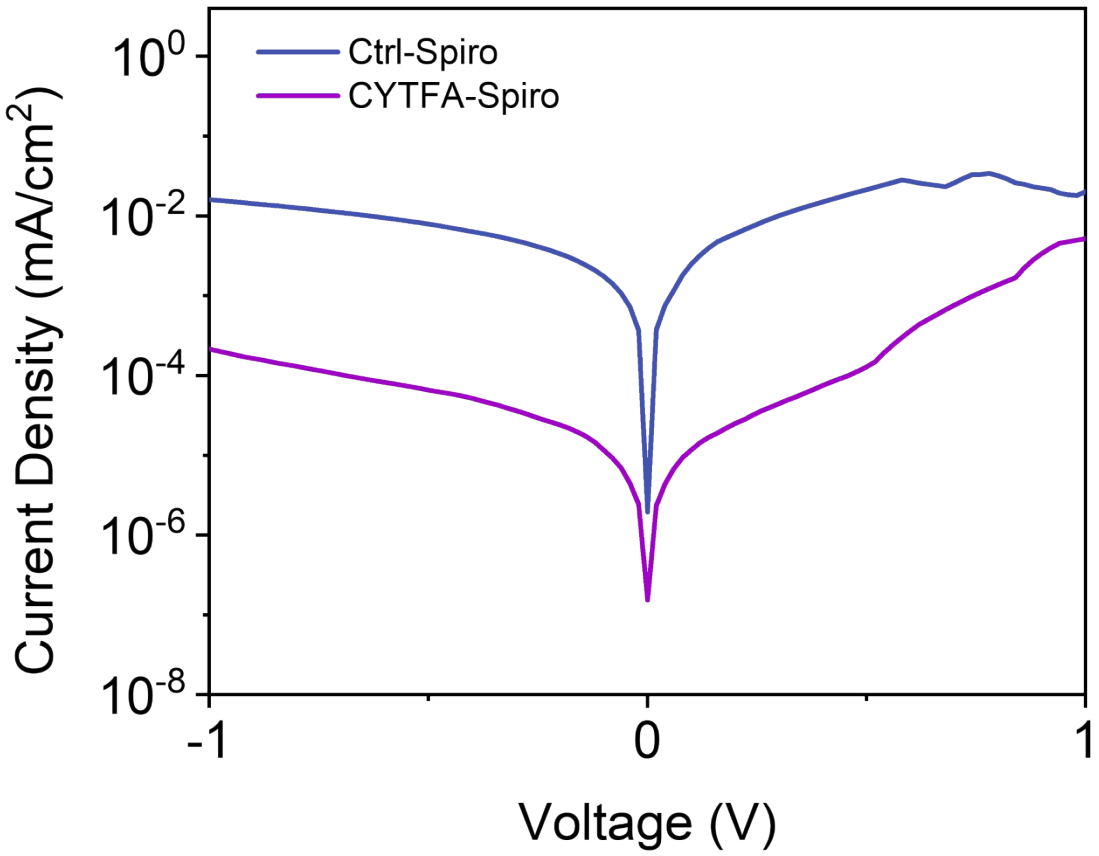

Fig. S16 Dark J-V curves of the Ctrl-Spiro and CYTFA-Spiro devices.

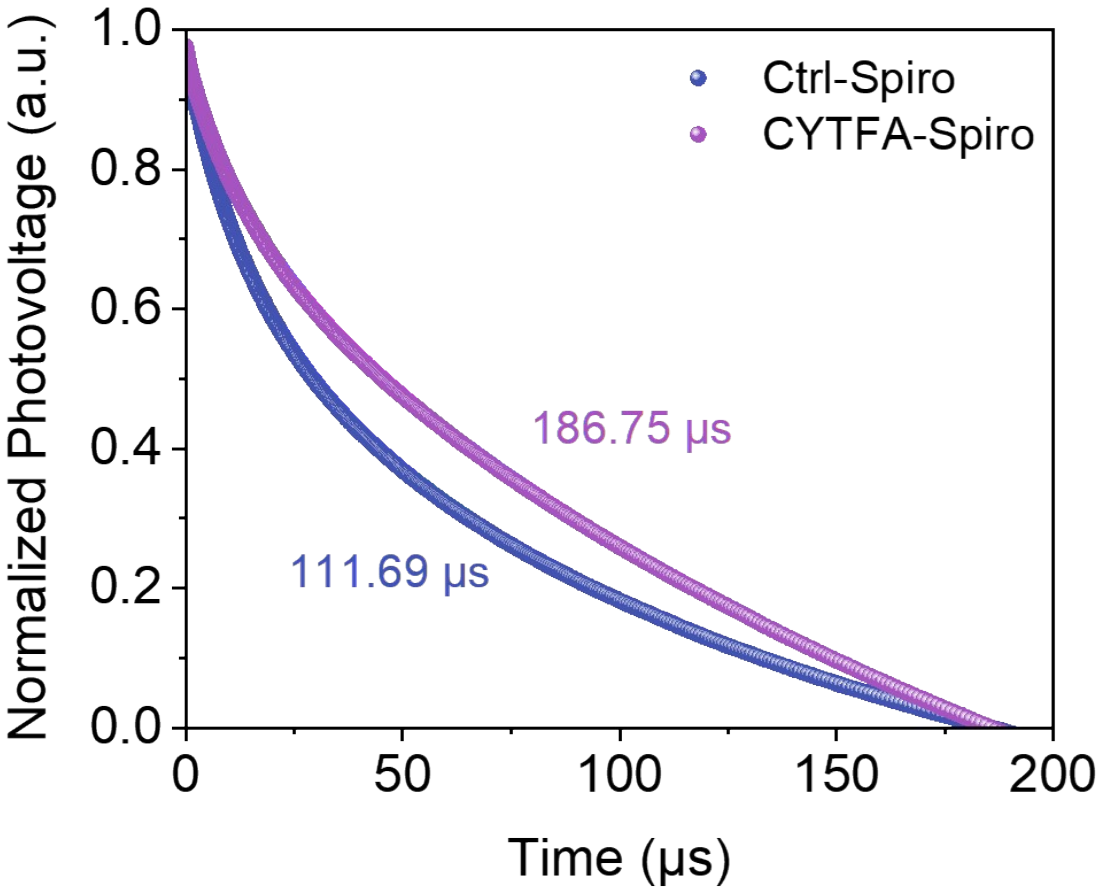

Fig. S17 TPV of the Ctrl-Spiro and CYTFA-Spiro devices with offset intensity at 8.5%.

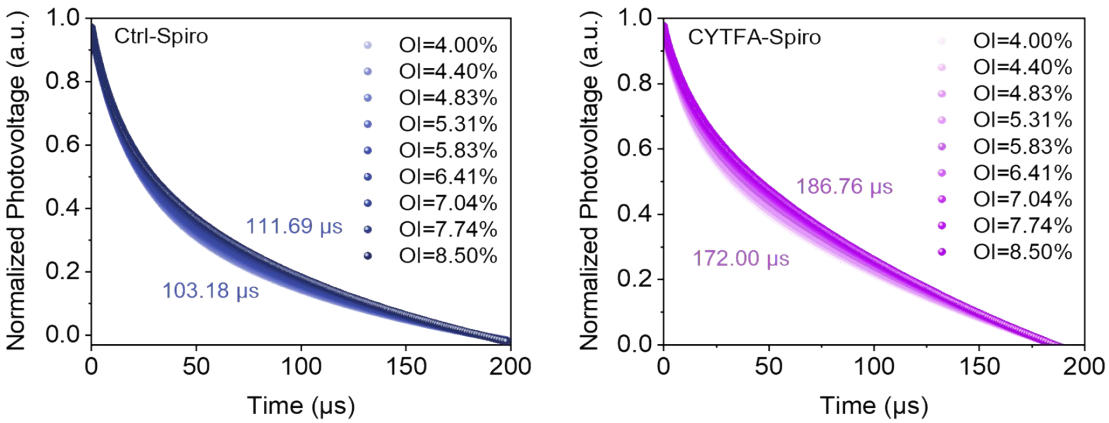

Fig. S18 TPV of the Ctrl-Spiro and CYTFA-Spiro devices with different offset intensity.

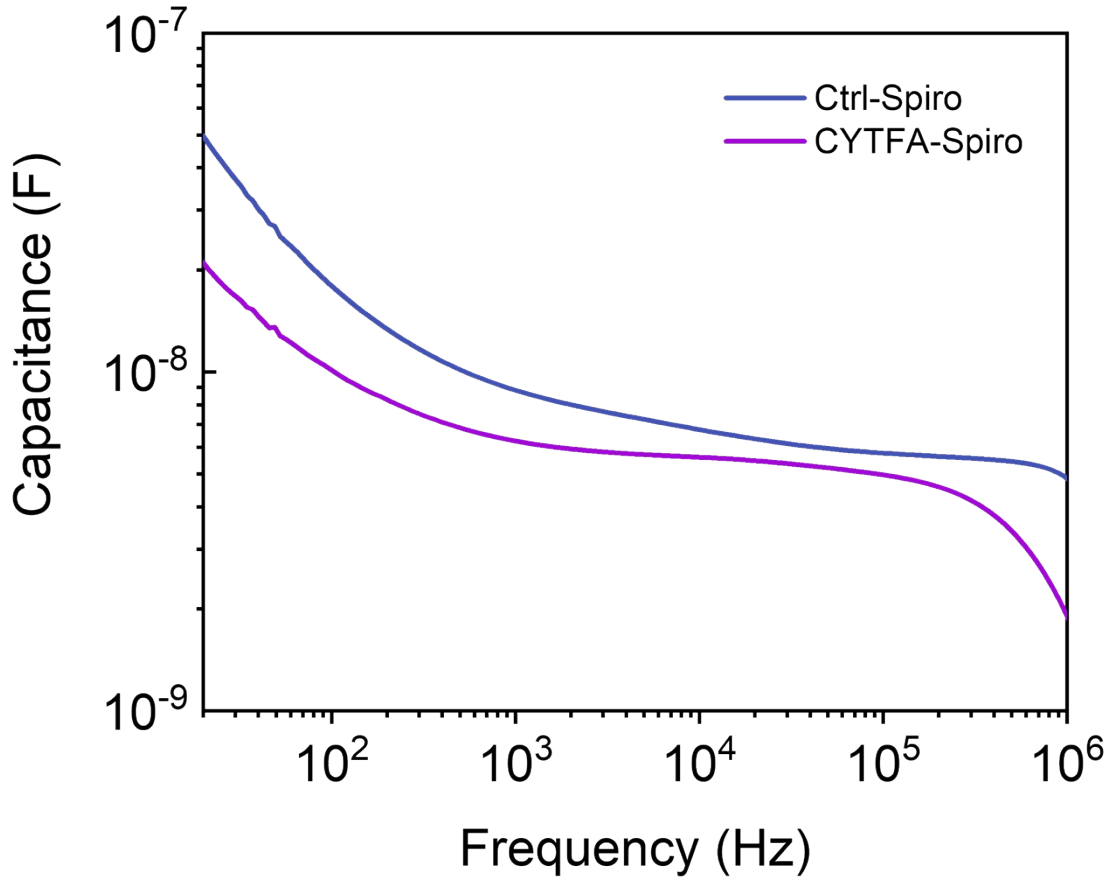

Fig. S19 Capacitance spectra of the Ctrl-Spiro and CYTFA-Spiro devices.

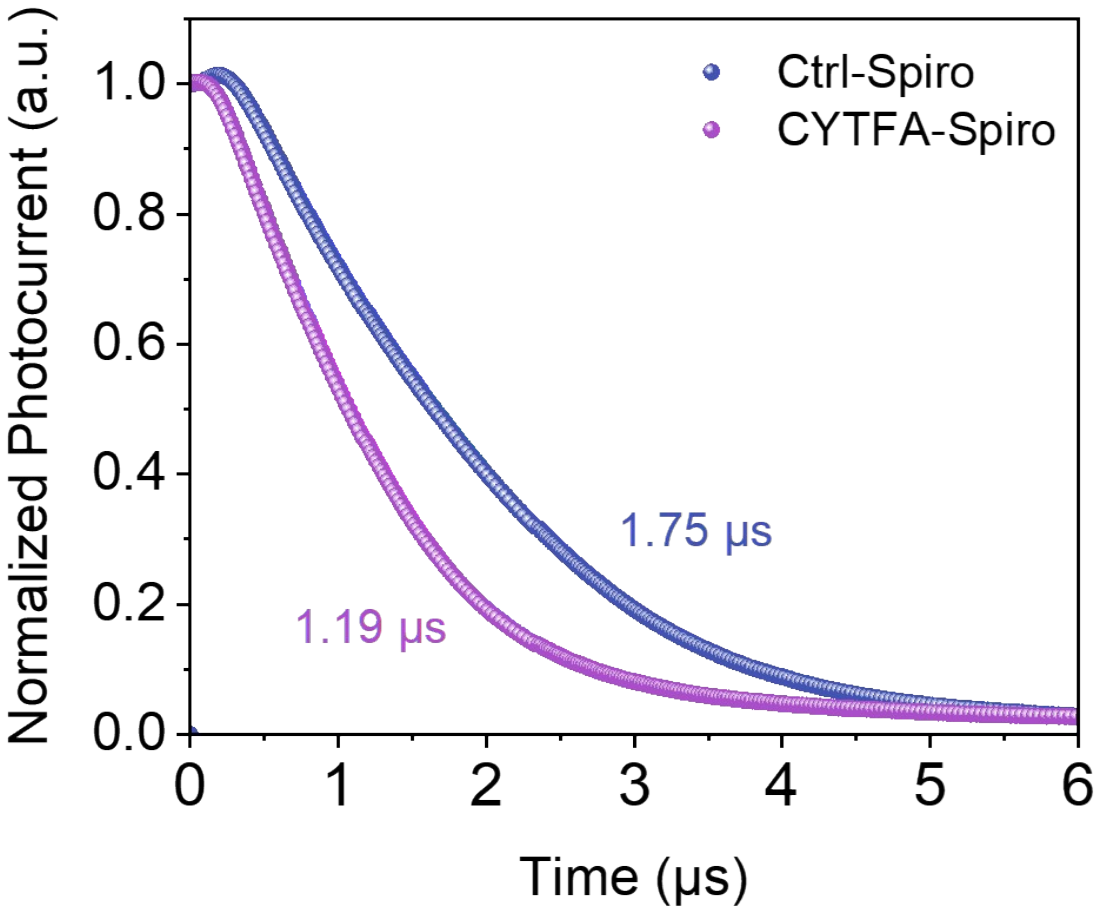

Fig. S20 TPC of the Ctrl-Spiro and CYTFA-Spiro devices with light intensity at 1.

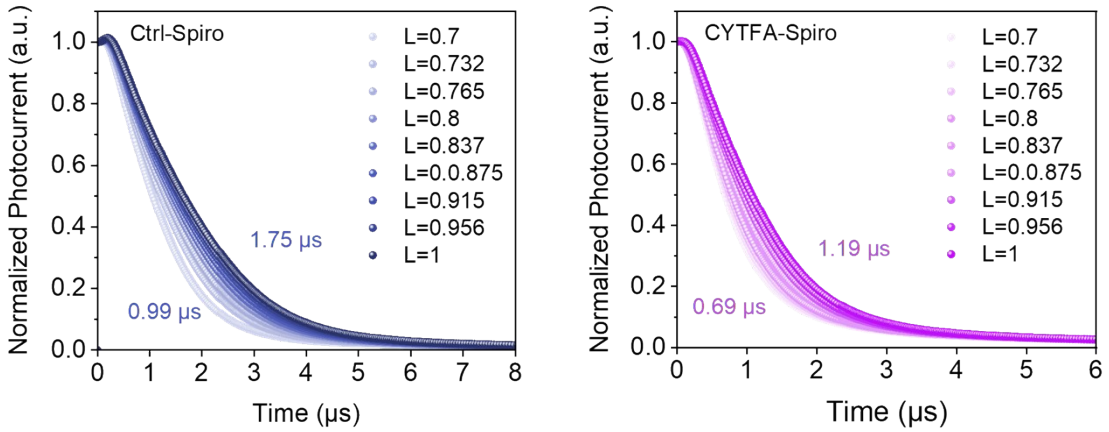

Fig. S21 TPC of the Ctrl-Spiro and CYTFA-Spiro devices with different light intensities.

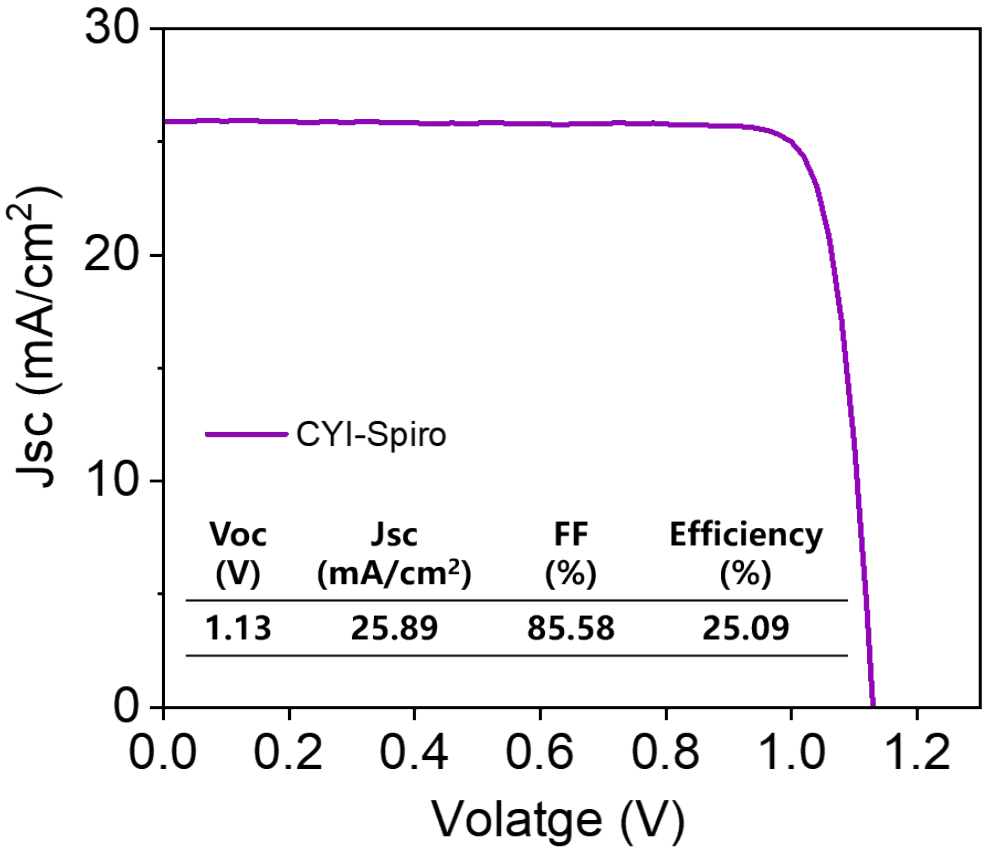

Fig. S22 Current density-voltage characteristics of the best performance of the CYI-Spiro device.

Table S1 Summary of doping systems with and without LiTFSI and TBP.

No LiTFSI and TBP doped system						
Molecular	**Architecture**	**PCE (%)**	**Jsc (mA/cm²)**	**Voc (V)**	**FF (%)**	**Ref.**
Spiro-OMeTAD$^{2\bullet+}$(TFSI$^-$)$_2$, 4-tert-butyl-1-methylpyridinium bis(trifluoromethylsulfonyl)imide	FTO/TiO_2/$FAPbI_3$/ Spiro-OMeTAD/Au	25.01	26.49	1.16	81.35	1
Tetrabutylammonium bis-(trifluoromethanesulfonyl)imide Tetrabutylammonium tetrafluoroborate	FTO/TiO_2/ $Rb_{0.05}Cs_{0.05}FA_{0.8}MA_{0.07}PbI_{2.57}Br_{0.4}$/ Spiro-OMeTAD/Au	18.4	22.3	1.07	77	2
Spiro-OMeTAD$^{2\bullet+}$(TFSI$^-$)$_2$, N,N,N′,N′-Tetrakis(4-methoxyphenyl)benzidine bis(trifluoromethanesulfonyl)imide	FTO/TiO_2/ $(FA)_{0.91}(MA)_{0.09}Pb(I_3)_{0.91}(Br_3)_{0.09}$/ Spiro-OMeTAD/Au	13.15	19.62	0.96	70	3
Spiro-OMeTAD$^{2\bullet+}$(TFSI$^-$)$_2$	FTO/TiO_2/ $Rb_{0.05}Cs_{0.05}FA_{0.8}MA_{0.07}PbI_{2.57}Br_{0.4}$/ Spiro-OMeTAD/Au	19.3	23.9	1.08	75	4
LiTFSI and TBP doped system						
molecular	**Architecture**	**PCE (%)**	**Jsc (mA/cm²)**	**Voc (V)**	**FF (%)**	**Ref.**
1-dodecanethiol	ITO/SnO2/ $Cs_{0.05}FA_{0.81}MA_{0.14}PbI_{2.55}Br_{0.45}$/ PMMA/spiro-OMeTAD /Au	23.1	24.6	1.15	81.13	5
CO_2	ITO/SnO2/ $Cs_{0.05}FA_{0.81}MA_{0.14}PbI_{2.55}Br_{0.45}$/ Spiro-OMeTAD/Au	19.1	21.2	1.14	79.00	6
12-crown-4	ITO/SnO2/ $Cs_{0.05}FA_{0.85}MA_{0.1}Pb(I_{0.97}Br_{0.03})_3$ / Spiro-OMeTAD/Au	23.23	24.97	1.14	81.35	7
ferrocene	FTO/SnO_2/$(FAPbI_3)_{0.99}(MAPbBr_3)_{0.01}$/ Spiro-OMeTAD/Au	23.45	25.26	1.153	80.50	8
1,6-diazidohexane	$Cs_{0.05}FA_{0.85}MA_{0.1}PbI_3$	22.7	24.7	1.17	76.00	9
Cyclohexylamine Trifluoroacetic acid (Our Work)	FTO/$FAPbI_3$/Spiro-OMeTAD/MoO_3/Au	25.8	26.14	1.17	84.10	

Table S2 The relative PL decay time (τ_{PL}), the estimated charge carrier transfer time (τ_{CT}) and efficiency (η) from the TRPL results

Perovskite materials	**Species**	**τ_{PL} (ns)**	**τ_{CT} (ns)**	**η (%)**
$FAPbI_3$	perovskite	3800		
	Perovskite/Ctrl- Spiro	65.89	67.05	98.27
	Perovskite/CYTFA-Spiro	12.37	12.41	99.68

Table S3 The parameters of champion devices based on Ctrl-Spiro and CYTFA-Spiro.

Devices	V_{OC} (V)	J_{SC} (mA/cm^2)	FF (%)	PCE (%)
Ctrl-Spiro	1.10	25.22	82.34	23.02
CYTFA-Spiro	1.17	26.14	84.10	25.80

References

1. T. K. Zhang, F. Wang, H. B. Kim, I. W. Choi, C. F. Wang, E. Cho, R. Konefal, Y. Puttisong, K. Terado, L. Kobera, M. Y. Chen, M. Yang, S. Bai, B. W. Yang, J. J. Suo, S. C. Yang, X. J. Liu, F. Fu, H. Yoshida, W. M. M. Chen, J. Brus, V. Coropceanu, A. Hagfeldt, J. L. Brédas, M. Fahlman, D. S. Kim, Z. J. Hu and F. Gao, *Science*, 2022, **377**, 495-501.
2. J. B. Zhang, T. Zhang, L. C. Jiang, U. Bach and Y. B. Cheng, *Acs Energy Letters*, 2018, **3**, 1677-1682.
3. W. Zhang, F. G. Zhang, B. Xu, Y. Y. Li, L. Q. Wang, B. B. Zhang, Y. Guo, J. M. Gardner, L. C. Sun and L. Kloo, *ACS Appl. Mater. Interfaces*, 2020, **12**, 33751-33758.
4. B. Tan, S. R. Raga, A. S. R. Chesman, S. O. Fürer, F. Zheng, D. P. McMeekin, L. C. Jiang, W. X. Mao, X. F. Lin, X. M. Wen, J. F. Lu, Y. B. Cheng and U. Bach, *Adv. Energy Mater.*, 2019, **9**, 10.
5. X. Liu, B. L. Zheng, L. Shi, S. J. Zhou, J. T. Xu, Z. H. Liu, J. S. Yun, E. Choi, M. Zhang, Y. H. Lv, W. H. Zhang, J. L. Huang, C. X. Li, K. W. Sun, J. Seidel, M. R. He, J. Peng, X. J. Hao and M. Green, *Nat. Photonics*, 2023, **17**, 96.
6. J. M. Kong, Y. Shin, J. A. Röhr, H. Wang, J. Meng, Y. S. Wu, A. Katzenberg, G. Kim, D. Y. Kim, T. D. Li, E. Chau, F. Antonio, T. Siboonruang, S. Kwon, K. Lee, J. R. Kim, M. A. Modestino, H. L. Wang and A. D. Taylor, *Nature*, 2021, **594**, 51-56.
7. Y. Shen, K. M. Deng, Q. H. Chen, G. Gao and L. Li, *Adv. Mater.*, 2022, **34**, 9.
8. T. Webb, X. P. Liu, R. J. E. Westbrook, S. Kern, M. T. Sajjad, S. Jenatsch, K. Jayawardena, W. H. K. Perera, I. P. Marko, S. Sathasivam, B. W. Li, M. Yavari, D. J. Scurr, M. R. Alexander, T. J. Macdonald, S. A. Haque, S. J. Sweeney and W. Zhang, *Adv. Energy Mater.*, 2022, **12**, 14.
9. Y. P. Han, G. Zhang, H. B. Xie, T. F. Kong, Y. H. Li, Y. Zhang, J. Song and D. Q. Bi, *Nano Energy*, 2022, **96**, 7.